A DYNAMIC MODEL FOR FLYWHEEL-BASED PIVOTING IN RECONFIGURABLE CUBIC MODULES

[1, 2, *] **Halil İbrahim DOKUYUCU** [iD], [3] **Nurhan GÜRSEL ÖZMEN** [iD]

[1] *Karadeniz Technical University, Graduate School of Natural and Applied Science, Trabzon, TÜRKİYE*
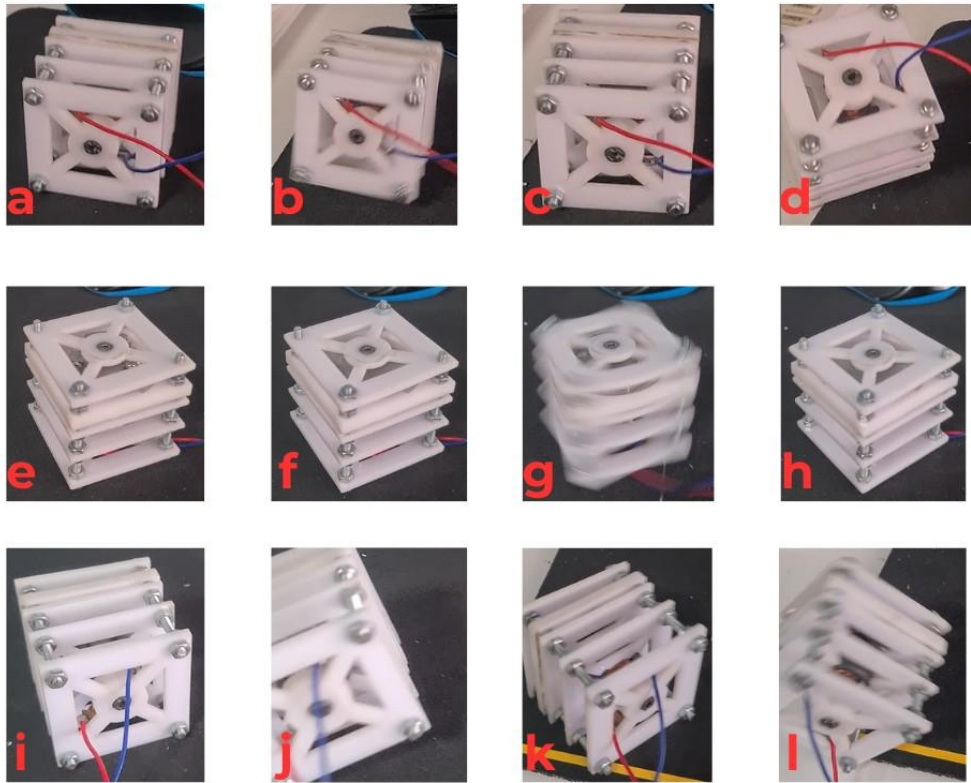[2] *Sanayi Mah. Devlet Karayolu Cad. Yaren Sokak No:1 Trabzon, TÜRKİYE*
[3] *Karadeniz Technical University, Mechanical Engineering Department, Trabzon, TÜRKİYE*
[1,2] halilibrahimdokuyucu@tiski.gov.tr, [3] gnurhan@ktu.edu.tr

Highlights

- A dynamic model for pivoting motion of a cubic shaped module.

- Actuation and braking systems are integrated into a single platform.

- Principle of angular momentum conservation is used.

- Pivoting motion is successfully achieved.

Graphical Abstract

The experiments of the pivoting motion

*Corresponding Author: Halil İbrahim DOKUYUCU, halilibrahimdokuyucu@tiski.gov.tr

A DYNAMIC MODEL FOR FLYWHEEL-BASED PIVOTING IN RECONFIGURABLE CUBIC MODULES

[1, 2, *] **Halil İbrahim DOKUYUCU** (iD), [3] **Nurhan GÜRSEL ÖZMEN** (iD)

[1] *Karadeniz Technical University, Graduate School of Natural and Applied Science, Trabzon, TÜRKİYE*
[2] *Sanayi Mah. Devlet Karayolu Cad. Yaren Sokak No:1 Trabzon, TÜRKİYE*
[3] *Karadeniz Technical University, Mechanical Engineering Department, Trabzon, TÜRKİYE*
[1,2]halilibrahimdokuyucu@tiski.gov.tr, [3]gnurhan@ktu.edu.tr

ABSTRACT: This paper introduces a dynamic model of a novel flywheel that provides a pivoting motion for a cubic module in reconfigurable systems. The challenges associated with pivoting motion for lattice-type self-reconfigurable modular robots are investigated, particularly the momentum-driven ones, where the existing models use two separated systems for actuation and braking. The proposed system allows a combined actuation and braking system, to manage the pivoting action. The mathematical model of the dynamical flywheel is developed according to Newton's Law. The flywheel has a variable diameter depending on the angular speed, where the sudden brake is applied by the collision between the flywheel end and the braking notch. The angular momentum transfer from the flywheel to the module body provides pivoting torque, which is the fundamental principle in momentum-driven systems. The dynamic model is verified by experimental studies. The experimental findings indicate that the success rates of the proposed system are 90% and 80% for traverse and horizontal traverse pivoting motion respectively. The average time duration for traverse and horizontal traverse pivoting motion are 0.906 and 0.763 seconds respectively. Based on the findings, the study indicates that the developed flywheel is a potential candidate for a pivoting actuator in the self-reconfigurable modular robotic field.

Keywords: Flywheel, Modular Robots, Pivoting Motion, Self-Reconfiguration, Variable Diameter

1. INTRODUCTION

A self-reconfigurable modular robot (SRMR) is defined as a robotic system consisting of a group of robotic modules that are interchangeable, autonomous, and communicative [1]. The main distinction of the SRMRs from the conventional robots is the shape changing capability [2]. Moreover, the interdependence of the module blocks can be regarded as the main difference from the multi-robot systems [3]. Modularity provides an adaptation capability to the robotic system in changing environmental conditions. Specialized modules, each with a distinctive connection mechanism, can be controlled together to perform a task based on a predefined configuration. The research on the field has emerged in the last decades with promising outcomes at challenging robotic missions in micro gravity [4], rough [5] and flat [6] terrains, aquatic [7], and aerial [8] environments. Versatility, reliability, and low-cost are the three main promises that the researchers have been following in the field [9]. Versatility, which can be defined as providing a wide range of tasks by using a single robotic system, is validated in the literature [1]. However, studies on reliability and low-cost promises are still conducted by the researchers to validate them [10].

Self-repair and fault-tolerance behaviors of SRMRs make them preferable in complex tasks such as space missions or hazardous environmental tasks where direct intervention is not possible. Reliability is not an easy goal to achieve when the number of the modules is high. High number of modules bring hardware and computational complexity. Therefore, the control system of a SRMR needs to be simple to reach the low-cost target. On the basis of the promises and advantages, a wide range of application areas for SRMRs have been studied in the literature such as water surveillance [11], space missions [4] [12], in-

---

*Corresponding Author: Halil İbrahim DOKUYUCU, halilibrahimdokuyucu@tiski.gov.tr

pipe inspection [13], cleaning of liquid tanks [14], and nuclear decommissioning and inspection [15].

SRMR studies form a collective foundation for advancing robotic systems, with several comprehensive reviews laying the groundwork for future research. Early works, such as [16], provided a fundamental classification of SRMRs based on module structural geometries and identified key emerging technological aspects, including automatic docking, configuration recognition, and distributed control. While offering a valuable broad overview of the field's technological landscape, this work primarily focused on general classification rather than detailed challenges or specific performance metrics. Subsequently, the review in [17] delved into a more specialized area, reviewing docking systems crucial for SRMR reconfiguration and providing a forward-looking vision for research specifically in module interconnection mechanisms. However, this review focused predominantly on the mechanical aspects of docking, without extensive discussion on the integrated control strategies or the generation of dynamic reconfigurable motions. Similarly, the review in [18] highlighted the significant advantages of bio-inspired SRMRs, emphasizing their adaptability and resilience. This review tended to concentrate on high-level conceptual benefits and potential applications rather than providing a detailed analysis of novel internal actuation mechanisms or specific design methodologies for achieving complex reconfigurations. Collectively, these foundational and specialized reviews mention the progress in SRMRs but also reveal a continued need for research that explores innovative internal mechanisms for precise and controlled reconfigurable movements. Addressing this critical gap, this study introduces a novel variable-diameter flywheel system, which, upon reaching a specific angular velocity, engages a notch to efficiently transfer angular momentum to the module body, thereby enabling controlled pivoting action for self-reconfiguration.

The main distinction between SRMRs and conventional robotic systems is that SRMRs have changeable shape formation. Modularity and motion capabilities of the modules provide this shape changing ability. Docking mechanisms enable the modules to stick on the main configuration, as well as to detach when needed. If all of the modules of an SRMR are identical, the system is called homogeneous [2], otherwise it is called heterogeneous [19].

The mechanical structure of an SRMR system is related to the relative positions of the modules, where biological inspirations have a leading role in defining the structural formation. The chain type, lattice type, and mobile structure of structural formations are frequently selected in the field [2]. Moreover, hybrid type, truss structure, and the free form are the other types of structures. The lattice type tries to mimic the water molecules whose flow pattern is an important inspiring factor in the field. The lattice is created by combining the modules in a multi directional order, as well as adding branches if necessary. The most important advantage of a lattice-type SRMR is flexible locomotion. When the modules encounter a confined space, they can easily separate from each other and perform critical tasks in inaccessible areas. One platform might offer benefits of water flow motion on rough terrains, flat terrains with obstacles, passing through narrow corridors or pipes, climbing stairs, and complex environments. Metamorphic [20], Atron [21], 3D M-Blocks [22], ModQuad [23], Catom 3D [24], and Electrovoxel [25] are among the leading validated examples of lattice-type SRMRs. Aerial working environment of ModQuad, momentum-driven actuation of 3D M-Blocks, and magnetic actuation of Electrovoxel have introduced novel aspects to the field.

The Pivoting Cube Model (PCM), Sliding Cube Model (SCM), Compressible Cube Model (CCM), and Module Carrier Model (MCM) have been proposed as motion models for lattice-type SRMRs in the field. PCM has emerged as a consistent module motion model [22], [25], [26], [27]. When compared to models such as the SCM [28], the CCM [29], and the MCM [30], PCM can be considered a more applicable model for real-world problems. The SCM is mostly applicable to two-dimensional problems due to the invalidated applicability of concave rotational motion [31]. Since achieving the sliding motion of a cubic module through an internal actuator requires a complex structure [32], these systems are generally actuated by external actuators, which significantly restricts the operational area to a very limited space [28], [31]. In the CCM, an efficient operation cannot be achieved due to the excessive time required for the expansion and compression steps of the cube surfaces [33]. In the MCM, the

inhomogeneous structure formed by the connection arms and cubic modules needs a double-layered process for the execution of commands sent by the controllers which increases the computational burden [30]. On the other hand, PCM is not restricted to two dimensions, can easily adapt to both internal and external actuators, and can be controlled with simple controller commands. One of the significant advantages provided by PCM is that modules do not always need to remain connected during movement. Therefore, in case of an external impact causing module separation, the modules can move independently and reconstruct the robotic configuration [22].

A novel approach utilizing momentum-driven systems as actuators for strong pivoting motion and using simple permanent magnets as docking mechanism has been introduced in [22]. In a module-embedded flywheel system, accelerating the flywheel generates significant torque. When abruptly halted by a braking mechanism, this torque transfers to the module body, enabling pivoting around a desired axis. However, in 3D M-Blocks robots, the actuation system driving the flywheel and the braking mechanism operate as separate components. This separation introduces spatial constraints and increases control complexity, presenting a limitation that remains open for further optimization.

This study proposes a dynamic model for a lattice-type self-reconfigurable modular robot (SRMR) that utilizes a novel actuation method based on momentum conservation, similar to existing approaches in the literature [22]. However, unlike previous designs, the proposed method introduces a variable-radius dynamic flywheel that stops abruptly by colliding with a barrier once it reaches a predetermined angular velocity. This design integrates both the drive and braking systems into a single structure, reducing complexity and spatial constraints. To the best of our knowledge, this is the first implementation of such an actuation mechanism in the literature.

This specific approach to generating dynamic reconfigurable motion also fundamentally distinguishes the proposed system from other prominent actuation mechanisms in modular robotics. For instance, while 3D M-Blocks [22] are highly versatile in achieving various articulated motions and complex reconfigurations through direct motor-driven joints and inter-module magnetic connections, their computation burden raises from controlling the pivoting and braking separately. Another example, Torque Capsules [34] employ an internal reaction wheel to generate continuous torque for precise attitude control or relatively slow angular repositioning of modules; the proposed system, in contrast, is purpose-built for a single, powerful burst of angular momentum to achieve a distinct pivoting motion. Furthermore, sophisticated systems like Cubli [35] uses multiple internal reaction wheels for dynamic balancing, jumping, and multi-axis control; however, its mechanism relies on continuous reaction torque against external surfaces or internal balancing, differing significantly from the proposed method's targeted internal momentum transfer through direct impact to achieve a module's pivoting on a surface. The proposed variable-diameter flywheel approach therefore offers a unique solution specifically designed for efficient and powerful pivoting actions, providing a distinct mode of self-reconfiguration within the modular robotics field.

The rest of this study is structured as follows: Section 2 details the proposed dynamic model for the modules. Section 3 presents the numerical and experimental results, along with a comparison to existing studies in the literature. Finally, Section 4 concludes the study and outlines directions for future research.

2. MATERIAL AND METHODS

This section, presents the development of a dynamic model for the pivoting motion of a cubic module. In Section 2.1, the coordinate systems that describe the direction of rotation of the flywheel and the pivoting motion of the module body are given. Then, in Section 2.2, the dynamic formulation representing the pivoting motion and its interaction with the flywheel is presented.

2.1. The Problem Setup and the Coordinate System Definition

Based on the design requirements of the SRMRs, the actuation system must be compact and capable

of fitting within a limited volume. A novel actuation system has been developed regarding the principle of conservation of angular momentum. The system generates angular momentum through the rotation of a flywheel, and when the flywheel is abruptly stopped, its angular momentum transfers to the module body, producing the torque required for pivoting motion. A three-dimensional representation of the actuation system's operating principle is shown in Figure 1.
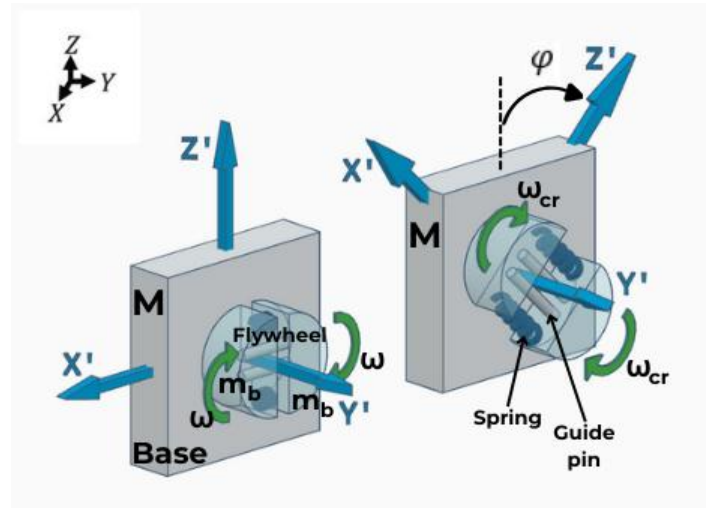

Figure 1. Visualization of the actuation system in 3D

In Figure 1, the flywheel consists of two equal masses, denoted as m_b , connected by two springs. Two identical shafts pass through the center of the flywheel components. As the flywheel accelerates to a certain angular velocity, the gap between its components increases, causing them to collide with a notch on the module body. In the figure, two coordinate systems are included: the global coordinate system (XYZ) and the local coordinate system ($X'Y'Z'$). The local coordinate system is attached to the flywheel, with the Z and Z' axes aligned. The flywheel is connected to the module body via a DC motor and has a single rotational degree of freedom about the Y'-axis, as indicated by the arrow in Figure 1. The actuation system ensures that the module pivots in either the clockwise (CW) or counterclockwise (CCW) directions, depending on the flywheel's angular velocity (ω). A positive (ω) induces CCW pivoting, whereas a negative (ω) results in CW pivoting. The angle φ, shown in Figure 1, represents the pivoting motion direction within the global coordinate system.

The actuation system operates on the principle that the radius of the flywheel changes due to the centrifugal force acting on its rotating identical components. This variation in radius causes the flywheel to collide with the notches on the module body, generating the pivoting motion. Let the mass of each rotating flywheel component be denoted as m_b, and the spring constant as k. The initial radius of the stationary flywheel is r_0, while the rotating flywheel's radius is defined as $r(t)$. The relationship between angular velocity and the dynamic flywheel radius has been analyzed in detail.

The rotational motion of the flywheel can be analyzed as a periodic motion, with intermittent collisions between the flywheel and the notch. These collisions continue until the desired pivoting motion is achieved. As a result, each collision transfers momentum from the flywheel to the module body. Figure 2 illustrates the sequence of collision cycles leading to the complete pivoting motion.
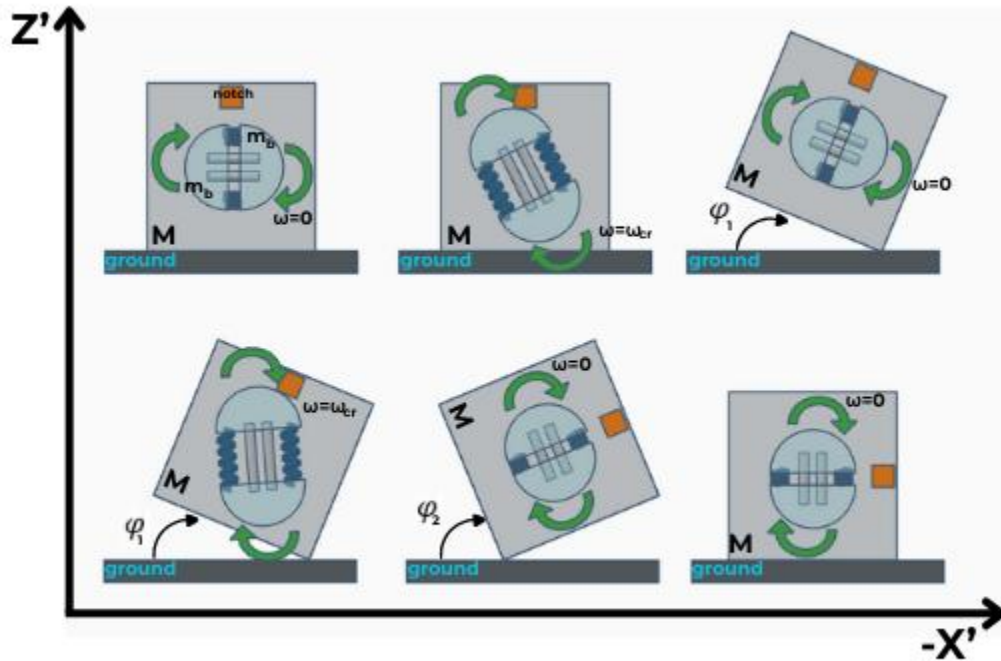
Figure 2. Conversion of angular rotational motion into pivot motion through two consecutive cycles

When the flywheel is stationary, it does not contact the notch. However, once the flywheel reaches a critical angular velocity (ω_{cr}), its radius increases, causing a collision between the flywheel and the notch. As a result of this collision, the angular position of the module body φ_1 changes. If this change is enough to complete the pivot motion, the flywheel is not reactivated. Otherwise, the collision cycles continue until the module body achieves full pivoting motion.

2.2. Dynamic Representation and Mathematical Model of the System

The full equation of motion for this system is obtained using Newton's Second Law of Motion. The flywheel is considered as a point mass. The mathematical model contains three movement types:
1-Translational motion of the flywheel parts (due to centrifugal force, spring tension, damping, and friction).
2- Rotational motion of the flywheel (angular acceleration due to torque from the motor).
3- Rotational motion of the outer cube (pivoting due to flywheel impact).
The free-body diagram (FBD) of the module is presented in Figure 3. The flywheel consists of two identical flywheel pairs. These pairs are connected by two helical springs. Additionally, two pins passing through the center enable movement.
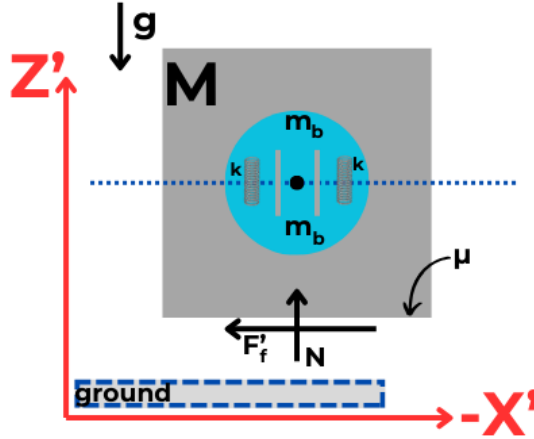
Figure 3. The free body diagram of the module

In Figure 3, total mass of the module and mass of a flywheel pair are denoted by M and m_b respectively. Normal and friction forces are denoted by N and F'_f respectively. Spring constant is denoted by k, whereas friction coefficient is denoted by μ. Finally, g denotes the gravity.

The spring constants are calculated as follows.

$$k = \frac{Gd^4}{8D^3T} \tag{1}$$

In Equation 1, G, d, D, and T represent the modulus of rigidity, diameter of the spring wire, spring diameter, and number of coils respectively.

1- Each flywheel pair moves outward under centrifugal force and is resisted by the spring, damping, and friction. During the translational motion of the flywheel, its pairs experience centrifugal force (F_u), spring force (F_s), and friction force (F_f) exerted by the guide pins. As the flywheel accelerates, its parts move outward, while negative acceleration causes the motion to move inward. Figure 4 illustrates the free-body diagram of a single flywheel part, along with the mass-spring-damper model for both flywheel pairs.

The equation of motion due to Newton's Second Law of Motion for a single flywheel pair is given in Equation 2,

$$m_b\ddot{r} + c\dot{r} + k(r - r_0) = m_b r \omega^2 - \mu N \tag{2}$$
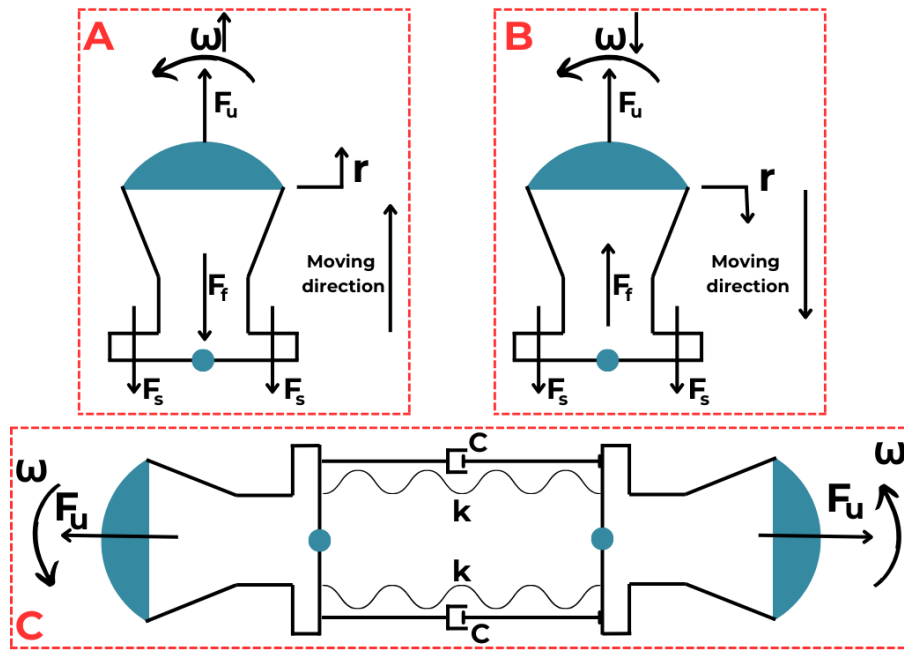
Figure 4. Free-body diagram of a single flywheel pair (A-B), mass-spring-damper model of both flywheel pairs (C)

When the flywheel collides with the notch, the voltage source turns the power off. As the flywheel stops rotating, flywheel parts return to the center due to the tensile forces of the springs. Upon re-energizing and the flywheel resumes rotation, and its pairs experience an outward centrifugal force. Once the angular velocity reaches a critical level, the centrifugal force overcomes the spring tension and friction forces, causing the flywheel components to move outward. During this movement, the spring tension increases, and at a critical point, a balance of forces is achieved. Figure 5 illustrates the flywheel states during the stationary and equilibrium velocity phases. r_0 is the initial radius of the flywheel, r is the dynamic radius of the flywheel, $r - r_0$ is the displacement due to motion.
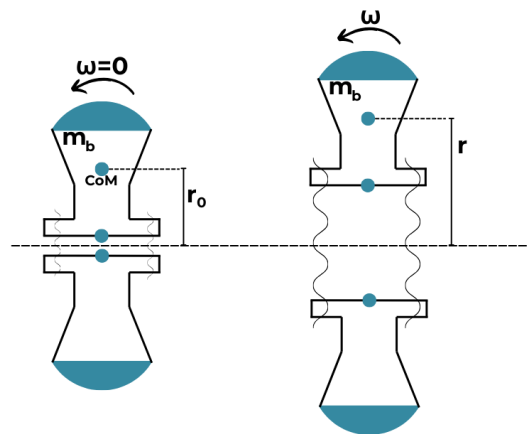
Figure 5. States of the flywheel components: stationary (left) and at equilibrium velocity (right)

On the right hand side of Equation 2, the centrifugal force acting on a flywheel pair during the accelerated rotational motion is defined as:

$$F_u = m_b r \omega^2 \tag{3}$$

On the left hand side of Equation 2, tension of the spring is expressed as:

$$F_s = k(r - r_0) \tag{4}$$

The effect of gravity on the centrifugal force varies depending on the position of the flywheel pair. The centrifugal force decreases for the upper flywheel pair. This effect is expressed in the following term:

$$T = m_b g \cos(\omega t) \tag{5}$$

The friction force includes Coulomb friction and viscous damping terms.

$$F_f = sign(\dot{r}) \times \mu N + c\dot{r} \tag{6}$$

The normal force (N) includes both the weight of the flywheel component and the rotational inertial force. Since the friction surface experiences a 360° displacement during rotation, the pattern of normal force due to gravity is a cosine function. The rotational inertial force, on the other hand, depends on the angular acceleration. Therefore, the friction force has been formulated as below:

$$F_f = \left(m_b r \dot{\omega} + m_b g \cos(\omega t)\right)\mu + c\dot{r} \tag{7}$$

The effect of gravity is considered negligible compared to the centrifugal force. The displacement term in Equation (7) can be replaced with the following expression.

$$r = \frac{m_b r_0 \omega^2}{(k - m_b \omega^2)} \tag{8}$$

The final form of the equation of motion of the flywheel can be described in Equation 9 based on the Newton's Second Law of Motion.

$$m_b \ddot{r} = m_b r \omega^2 - k(r - r_0) - m_b \mu \left(\frac{m_b r_0 \omega^2}{(k - m_b \omega^2)}\right)\dot{\omega} - c\dot{r} \tag{9}$$

In right side of Equation 9, the first term represents the centrifugal force, the second term denotes the spring tension, the third term corresponds to the friction force, and the fourth term represents the viscous damping.

The linearization of the derived equation of motion has been performed by using a Taylor series expansion. The linearization is applied to Equation 2 as below:

$$\frac{\partial(m_b \ddot{r})}{\partial \ddot{r}} \Delta \ddot{r} + m_b \ddot{r}_1 \tag{10}$$
$$= \frac{\partial F_u}{\partial \omega} \Delta \omega + \frac{\partial F_u}{\partial r} \Delta r + F_u(\omega_0, r_1) - \frac{\partial F_u}{\partial r} \Delta r - F_s(r_1) - \frac{\partial F_f}{\partial \dot{r}} \Delta \dot{r} - \frac{\partial F_f}{\partial \dot{\omega}} \Delta \dot{\omega}$$
$$- F_f(\dot{\omega}_0, \dot{r}_1)$$

In Equation 10, the expansion point of the Taylor series is given as (ω_0, r_1). The following expression can also be added to Equation 10.

$$m_b \ddot{r}_1 = F_u(\omega_0, r_1) - F_s(r_1) - F_f(\dot{\omega}_0, \dot{r}_1) \tag{11}$$

The Equations 10 and 11 can be combined as below:

$$\frac{\partial(m_b \ddot{r})}{\partial \ddot{r}} \Delta \ddot{r} = \frac{\partial F_u}{\partial \omega} \Delta \omega + \frac{\partial F_u}{\partial r} \Delta r - \frac{\partial F_u}{\partial r} \Delta r - \frac{\partial F_f}{\partial \dot{r}} \Delta \dot{r} - \frac{\partial F_f}{\partial \dot{\omega}} \Delta \dot{\omega} \tag{12}$$

Equation 12 can be defined as the linearization equation. General equation of motion and the linearization equation are combined as below:

$$m_b \Delta \ddot{r} + C \Delta \dot{r} + (k - m_b \omega_0^2) \Delta r = r \times (2 m_b \omega_0 \Delta \omega - m_b \mu \Delta \dot{\omega}) \tag{13}$$

The transfer function of the system is gained by using Equation 13 to control the displacement of the flywheel part.

$$\frac{R(s)}{\Omega(s)} = \frac{r(2\omega_0 - \mu s)}{s^2 + \dfrac{c}{m_b} s + \left(\dfrac{2k}{m_b} - \omega_0^2\right)} \tag{14}$$

The transfer function will be used to investigate the dynamic motion performance of the flywheel part considering the balance point of (ω_0, r_1). The state space representation of the system is given below:

$$\begin{bmatrix} \dot{z}_1 \\ \dot{z}_2 \end{bmatrix} = \begin{bmatrix} 0 & 1 \\ \omega_0^2 - \dfrac{2k}{m_b} & -\dfrac{c}{m_b} \end{bmatrix} \begin{bmatrix} z_1 \\ z_2 \end{bmatrix} + \begin{bmatrix} 0 \\ 1 \end{bmatrix} \omega \tag{15}$$

$$r = r[2\omega_0 \quad -\mu] \begin{bmatrix} z_1 \\ z_2 \end{bmatrix} \tag{16}$$

In Equation 16, the state variables are denoted as z_1 and z_2. The system input, angular velocity, and output, the displacement of the flywheel part, are denoted as ω and r respectively.

Once the mass of the flywheel part, which is related to the part dimensions, is determined, there are two adjustable parameters, viscous damping coefficient (c) and spring constant (k), in the system.

The natural frequency and damping coefficient of the system are given below:

$$\omega_n = \sqrt{\frac{2k}{m_b} - \omega_0^2} \tag{17}$$

$$\xi = \frac{c}{2m_b \sqrt{\dfrac{2k}{m_b} - \omega_0^2}} \tag{18}$$

Equations 17 and 18 can be rewritten as below, considering the displacement constraint:

$$\omega_n = \sqrt{\frac{\omega_0^2 r}{r_1} - \omega_0^2} \tag{19}$$

$$\xi = \frac{c}{2m_b \sqrt{\frac{\omega_0^2 r}{r_1} - \omega_0^2}} \tag{20}$$

As it is observed in Equation 19, the natural frequency of the system is directly related to r_1, x_0, x_1. Damping coefficient (ξ) is inversely proportional to the mass of the flywheel part and directly proportional to the viscous damping coefficient (c). To achieve the optimal damping coefficient ($\xi = 0.707$), the system must adhere to the following rule.

$$c = m_b \sqrt{\frac{2\omega_0^2 r}{r_1} - 2\omega_0^2} \tag{21}$$

The system gain is dependent on the flywheel dimensions, and shown in Equation 22. Once the flywheel dimensions are determined, the system gain becomes constant.

$$K_1 = \frac{2r\omega_0}{\frac{2k}{m_b} - \omega_0^2} \tag{22}$$

Viscous damping is directly related to the air friction applied to the flywheel pairs. The step response and the Bode diagram of the system with different viscous damping coefficients are shown in Figure 6. As the viscous damping between the flywheel part and the pin it moves on increases, the system's oscillation amplitude and overshoot decrease. In this case, the peak value of the frequency response also decreases. Therefore, it is observed that viscous damping is significant for the system. On the other hand, low viscous damping will increase vibrations in the system.

The steady-state condition for the flywheel motion is also investigated. At equilibrium ($\ddot{r} = 0, \dot{r} = 0$):

$$k(r_{eq} - r_0) = m_b r_{eq} \omega^2 - \mu N \tag{23}$$

Solving for r_{eq}:

$$r_{eq} = \frac{m_b \omega^2 r_0 + \mu N}{k - m_b \omega^2} \tag{24}$$

The denominator in Equation 24 determines the system's response:

* If $k > m_b \omega^2$, the system is stable, and r_{eq} is well defined.

* If $\omega > \omega_{cr} = \sqrt{k/m_b}$, the denominator approaches to zero, leading to instability and rapid expansion of the flywheel pairs.

When calculating the flywheel's total inertia, two flywheel pairs are considered together. Since the inertia values of the coupling element connecting the flywheel pairs to the motor shaft, springs, and pins are very low, they are neglected. The inertia of the flywheel is shown below:

$$I_f = 2 \times m_b \times r^2 \tag{25}$$
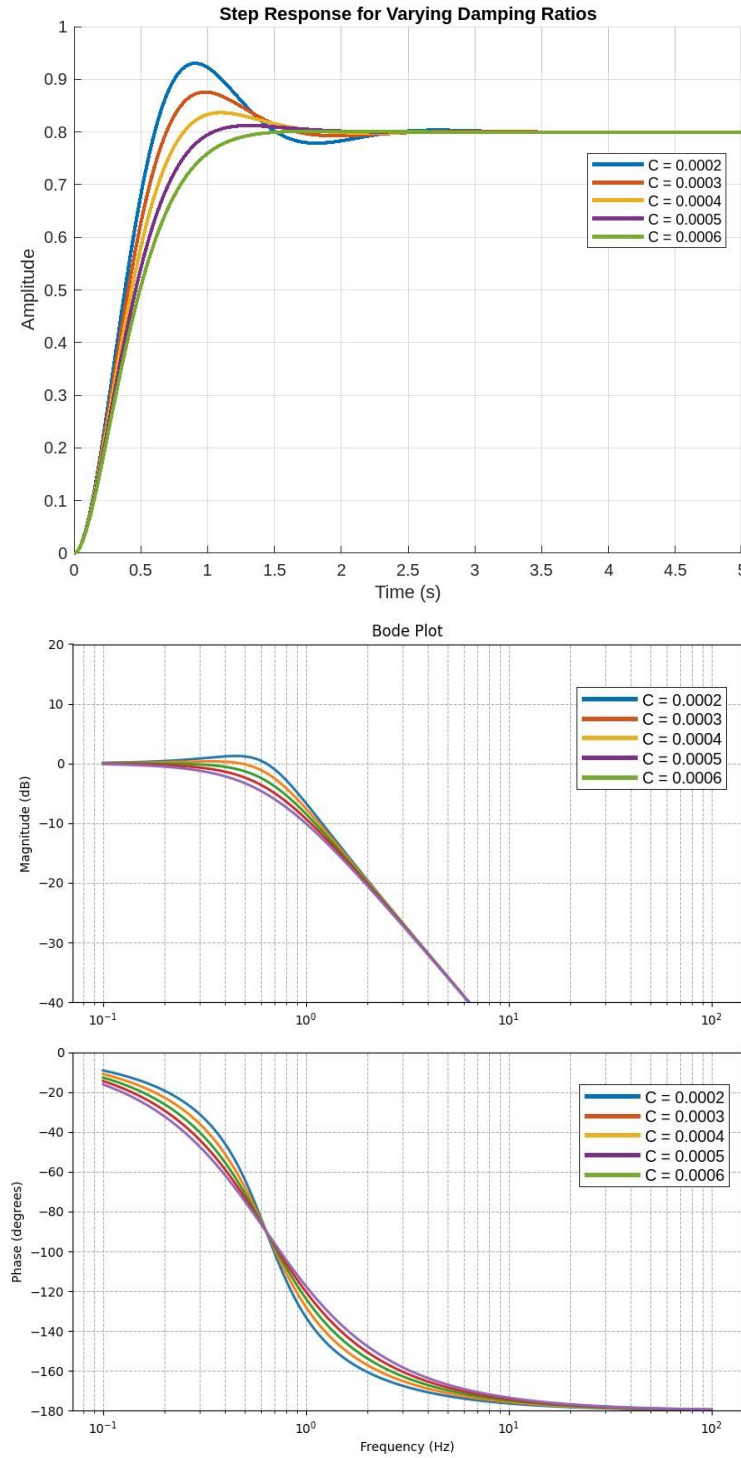
Figure 6. The step response (top) and Bode diagram (middle and bottom) of the system for different viscous damping coefficients

2- The rotating flywheel actuates the pivoting motion of the module. Using Newton's Second Law for rotational motion, the torque of the flywheel when it hits the notch (i.e. $\omega = \omega_{cr}$) is described as follows:

$$I_f \dot{\omega} = \tau_m - \tau_b - \tau_f \tag{26}$$

In Equation 26, I_f, $\dot{\omega}$, τ_m, τ_b, τ_f denote moment of inertia of the flywheel, angular acceleration, motor torque, braking torque, and friction torque respectively. The braking torque is zero since there is no extra braking mechanism in the system. When the flywheel suddenly stops due to braking, the torque transfer occurs as:

$$\tau_{impact} = \frac{I_f \Delta \omega}{\Delta t} \tag{27}$$

3- Rotational motion of the outer cube due to flywheel impact. When the flywheel abruptly stops rotating due to the impact with the notch. The impact method proposed in this study provides the same effect of decelerating a flywheel by a braking mechanism introduced in [22]. The energy stored in the flywheel is released in less than 15 ms, such that an impulse of torque is created. Therefore, the torque generated by the flywheel is transferred to the module body as shown in the below equation. This is the pivoting torque of the module as depicted in Figure 7.

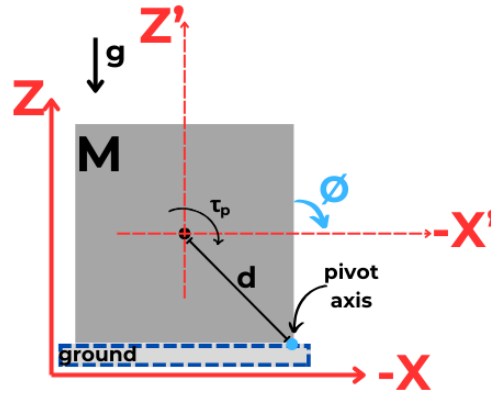$$\vec{\tau}_p = \vec{\tau}_{impact} \tag{28}$$

Figure 7. The resulting pivoting torque

Based on the angular momentum transfer mechanism, the pivoting torque is created about the axis through the center of gravity of the module. However, the stationary position of the module enforces it to rotate about the pivot axis shown in Figure 7. When studying multiple module lattice configurations, the magnetic bonding force will help to stabilize the pivot axis. Parallel axis theorem helps to calculate the moment of inertia about the pivot axis. The resulting pivoting torque must overcome magnetic bonding force and gravity in a lattice configuration. In this study, a single module movement is investigated. Therefore, the bonding resistance is not in the scope. The angular motion of the module due to the pivoting torque is described as follows based on the Newton's Second Law of Motion:

$$I_c \ddot{\varphi} + b \dot{\varphi} = \tau_p \tag{29}$$

In Equation 29, I_c, $\ddot{\varphi}$, b denote moment of inertia of the cube, angular acceleration of the cube, damping coefficient respectively.

It is observed that the angular position of the module is time-dependent and nonlinear. One should minimize the mass and moment of inertia, while maximizing the pivoting torque to provide a powerful pivoting motion. These parameters should be balanced during the design phase.

Bringing all the equations of motion for radial expansion of flywheel pair, flywheel rotation, and cube rotation:

$$m_b\ddot{r} + c\dot{r} + k(r - r_0) = m_b r\omega^2 - \mu N \tag{30}$$

$$I_f\dot{\omega} = \tau_m - \tau_b - \tau_f \tag{31}$$

$$I_c\ddot{\varphi} + b\dot{\varphi} = \tau_p \tag{32}$$

3. RESULTS AND DISCUSSION

Based on the derived dynamic model, relevant experimental studies have been conducted. A preliminary prototype is constructed for the tests. In the experiments conducted with the actuator placed in the core of the constructed module, the pivoting motion was successfully achieved.

3.1. Prototype of the Module

In this subsection, the resulting module prototype is presented briefly. A single cubic module with 60 mm edges were manufactured by using a 3D Printer (Prusa i3 MK3 with accuracy of $\pm0.015\ mm$). The material of the module body is selected as Polylactic Acid (PLA). The module includes thirty-six spherical permanent magnets (each having a diameter of 4.5 mm, nickel-coated, with a strength of Neodymium 35) to provide the face and hinge bonds during rest and pivoting. Three spherical magnets are mounted inside special cells separately on each edge, where they have enough space in the cells to rotate freely. The rooms are closed by using square hollow guides machined by using Plexiglas. Additionally, flywheel parts were produced by melting lead blocks and casting them into molds. The connection of these parts are maintained by using two cylindrical pins. The springs are attached from the outer sides of the flywheel parts. After finishing the fabrication process, a single prototype is produced as shown in Figure 8.
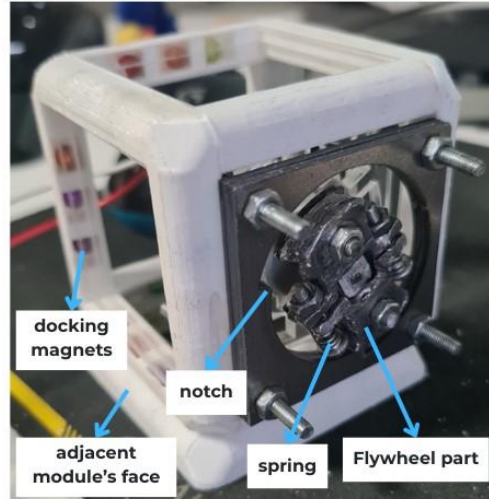

Figure 8. Module body and the flywheel
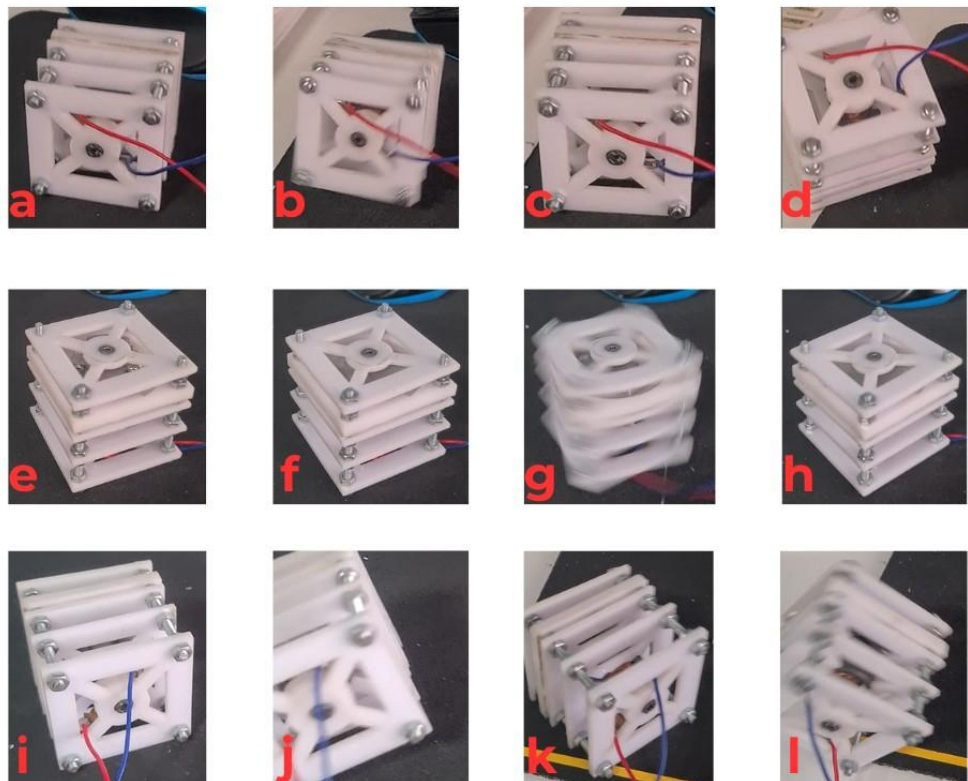
3.2. Pivoting Motion Experiments

Based on the produced prototype, pivoting motion experiments are conducted. As this study is mainly focusing on the dynamic model, the pivoting motion experiments are performed by the core structure of the modules. In the future work, the core structure and the module body will be integrated as a single platform. The experiment results are promising for further improvements of an SRMR to be

developed for a specific task such as field exploration in hazardous environments. In Figure 9, three sets of experiments are shown. Based on different axes, pivoting motions are achieved.

As it is seen in Figure 9, three different pivot motions are observed. When the flywheel is in the vertical position, during the movements between (a) and (d), the module attempts to perform a pivoting motion but rotates around a different axis, causing the flywheel to flip over to the horizontal position. When the flywheel is in the horizontal position, sudden braking successfully achieves the pivoting motion (e)-(h). When the flywheel is in the vertical position, the generated angular momentum proves sufficient, and a successful pivoting motion is achieved (i)-(l).

Based on the produced prototype, an initial comparison to a validated example from the literature, 3D M-Blocks [22] is shown in Table 1. In Table 2, pivoting motion performance metrics are compared to 3D M-Blocks [22]. Success rate is determined as the performance metric. It is observed that the success rates for traverse and horizontal traverse pivoting motion of the proposed module are 90% and 80% respectively. These rates are comparable with the 3D MBlocks. The slight difference from 3D MBlocks is that pivoting motion experiments in this study are conducted for individual modules on a flat ground. The comparison values in the tables offer encouraging insights for future developments.

Figure 10 shows the angular displacement as a function of pivoting motion duration for traverse and horizontal traverse pivoting motions. The average angular displacement for each pivoting motion is represented by a solid curve, while the surrounding shaded region depicts the results of 20 different trials. All pivoting actions consistently initiate from 0 and reach a final angular displacement of 90 degrees. The average time duration for the horizontal traverse motion is 0.763 seconds, which is slightly shorter than the average 0.906 seconds observed for the traverse pivoting motion. This difference is due to lower power requirements for horizontal movement, allowing for faster completion.

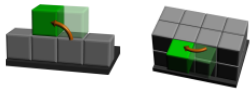**Figure 9.** The experiments of the pivoting motion
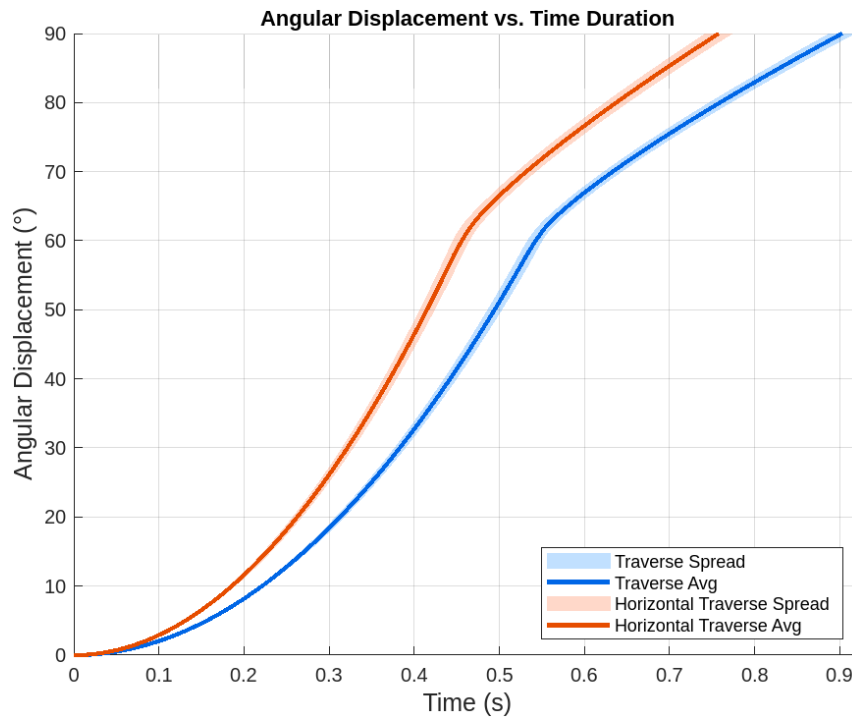
Figure 10. Angular displacement versus time duration of pivoting motion

Table 1. Comparison of the proposed module to 3D M-Blocks [22]

	Proposed Module	3D M-Blocks
Actuation Directions	1	6
Mass	82 g	150 g
Flywheel Moment of Inertia	7.2 E-6 kgm²	8.4 E-6 kgm²
Estimated Cost	$ 35	$ 130
Maximum Torque	1.4 Nm	2.6 Nm

Table 2. Comparison of the performance metrics of the proposed module to 3D M-Blocks [22]

	Proposed Module	3D M-Blocks
Illustrations (Traverse | Horizontal Traverse)		
Attempted	20 | 20	20 | 20
Success Rate	90% | 80 %	100% | 70%

4. CONCLUSIONS

SRMRs have emerged in the field of robotics over the past decades due to their promising advantages, particularly in confined spaces. The dynamic reconfiguration capability makes SRMRs superior to conventional rigid and mobile robots in inaccessible environments. Momentum-driven actuation mechanisms play a crucial role in the development of lattice-type SRMR modules capable of performing a pivoting motion individually. This individual pivoting motion provides advantages especially in field exploration tasks. The validated examples in the literature usually utilize separate mechanisms for actuation and braking systems, which increases complexity in terms of control. Therefore, this study presents a dynamic model for a novel flywheel design that integrates both

actuation and braking systems into a single platform. The mathematical model is derived using Newton's Second Law of Motion and the dynamic model is tested through experiments using a preliminary prototype. The pivoting motion is achieved in a single pivoting axis. Success rates of traverse and horizontal traverse pivoting motion are performance metrics. According to the experimental studies, the success rates are recorded as 90% and 80% for traverse and horizontal traverse pivoting motion respectively. These rates show that the proposed pivoting motion mechanism is a valid method that needs to further enhanced by appropriate adjustments.

While this study successfully introduces and models a novel variable-diameter flywheel mechanism for a pivoting motion, it is important to acknowledge some limitations of the current model and its conceptualization, which will serve as a basis for future improvements.

Firstly, regarding stability, the current pivoting mechanism focuses on generating the necessary momentum for pivoting. However, achieving precise landing and immediate post-pivoting stability presents challenges that require advanced control strategies, such as active damping or steering. The high-velocity impulsive nature of the angular momentum transfer can lead to residual oscillations that need to be actively managed for a stable final state.

Additionally, mechanical losses are an inherent factor in the angular momentum transfer process. Despite the success rate of the proposed pivoting mechanism, energy dissipation occurs due to inelastic collisions at the notch. Quantifying and minimizing these losses will be crucial for maximizing the energy efficiency in future iterations.

Finally, the durability of components, specifically the internal notch and the flywheel's surface, is a critical consideration for long-term operation. The repetitive, high-impact forces generated during angular momentum transfer induce significant stress on these parts. Future studies will include material testing and fatigue analysis to ensure the robust design and selection of materials that can withstand long-term operation. Addressing these limitations will be key to improving the core structure towards full module integration and practical application.

Declaration of Ethical Standards

The paper is prepared in accordance with ethical standards.

Credit Authorship Contribution Statement

Halil İbrahim DOKUYUCU and Nurhan GÜRSEL ÖZMEN equally worked on Conceptualization, Methodology, Software, Manufacturing, Validation, Formal analysis, Investigation, Writing – original draft, and Writing – review & editing.

Declaration of Competing Interest

The authors declare that they have no known competing financial interests or personal relationships that could have appeared to influence the work reported in this paper.

Funding / Acknowledgements

Data Availability

All data generated or analyzed during this study are included in this published article.

REFERENCES

[1] M., Yim, W.M., Shen, B., Salemi, D., Rus, M., Moll, H., Lipson, E., Klavins, and G.S. Chirikjian, "Modular self-reconfigurable robot systems [grand challenges of robotics]," *IEEE Robotics and Automation Magazine*, vol. 14, no. 1, pp. 43–52, March 2007, doi: 10.1109/MRA.2007.339623.

[2] H.İ., Dokuyucu and N., Gürsel Özmen, "Achievements and future directions of self-reconfigurable modular robots," *Journal of Field Robotics*, vol. 40, no. 3, pp. 701-746, May 2023, doi: 10.1002/rob.22139.

[3] M., Rubenstein, A., Cornejo, and R., Nagpal, "Programmable selfassembly in a thousand-robot swarm," *Science*, vol. 345, no. 6198, pp. 795–799, Aug. 2014, doi: 10.1126/science.1254295.

[4] M., Goeller, J., Oberlaender, K., Uhl, A., Roennau, and R., Dillmann, 2012. "Modular robots for on-orbit satellite servicing," in *IEEE International conference on robotics and biomimetics (ROBIO)*, Guangzhou, China, 2012, pp. 2018-2023, doi: 10.1109/ROBIO.2012.6491265.

[5] Y., Özkan-Aydin and D.I., Goldman, "Self-reconfigurable multilegged robot swarms collectively accomplish challenging terradynamic tasks," *Sci. Robot.*, vol. 6, July 2021, Art. no. eabf1628, doi: 10.1126/scirobotics.abf1628.

[6] J.W., Romanishin, K., Gilpin, S., Claici, and D., Rus, "3D M-Blocks: Self-reconfiguring robots capable of locomotion via pivoting in three dimensions," in *IEEE International Conference on Robotics and Automation*, Seattle, WA, 2015, pp. 1925-1932, doi: 10.1109/ICRA.2015.7139450.

[7] G., Knizhnik and M., Yim, "Design and experiments with a low-cost single-motor modular aquatic robot", in *17th International conference on ubiquitous robots (UR)*, Kyoto, Japan, 2020, pp. 233-240, doi: 10.1109/UR49135.2020.9144872.

[8] R., Oung and R., D'Andrea, "The distributed flight array: design, implementation, and analysis of a modular vertical take-off and landing vehicle," *The International Journal of Robotics Research*, vol. 33, no. 3, March 2014, pp. 375–400, doi: 10.1177/0278364913501212.

[9] M., Yim, D.G., Duff, and K.D., Roufas, "PolyBot: a modular reconfigurable robot," in *Proceedings of the IEEE International conference on robotics and automation*, San Francisco, CA, USA. New York: IEEE, 1, April 2000, pp. 514–520. doi: 10.1109/robot.2000.844106.

[10] M.R., Jahanshahi, W.M., Shen, T.G., Mondal, M., Abdelbarr, S.F., Masri, and U.A., Qidwai, "Reconfigurable swarm robots for structural health monitoring: a brief review", *International Journal of Intelligent Robotics and Applications*, vol. 1, no. 3, Sep. 2017, pp. 287–305, doi:10.1007/s41315-017-0024-8.

[11] J., Paulos, N., Eckenstein, T., Tosun, J., Seo, J., Davey, J., Greco, V., Kumar, and M., Yim, "Automated self-assembly of large maritime structures by a team of robotic boats," *IEEE Transactions on Automation Science and Engineering*, vol 12, no. 3, July 2015, pp. 958–968, doi: 10.1109/TASE.2015.2416678

[12] J.A., Fulton and H., Schaub, "Forward dynamics analysis of origami-folded deployable spacecraft structures," *Acta Astronautica*, vol. 186, Sep. 2021, pp. 549–561, doi: 10.1016/j.actaastro.2021.03.022

[13] M., Ciszewski, T., Buratowski, M., Giergiel, P., Małka, and K., Kurc, "Virtual prototyping, design and analysis of an in-pipe inspection mobile robot," *Journal of Theoretical and Applied Mechanics (Poland)*, vol. 52, no. 2, April 2014, pp. 417–429.

[14] T., Fukuda and S., Nakagawa, "Approach to the dynamically reconfigurable robotic system," *Journal of Intelligent and Robotic Systems*, vol. 1, no. 1, March 1988, pp. 55–72, doi: 10.1007/BF00437320.

[15] W., Lee, M., Hirai, and S., Hirose, "Gunryu III: reconfigurable magnetic wall-climbing robot for decommissioning of nuclear reactor," *Advanced Robotics*, vol. 27, no. 14, June 2013, pp. 1099–1111, doi: 10.1080/01691864.2013.812174.

[16] D., Bao, X., Wang, H., Huang, and B., Liang, "Review of modular selfreconfigurable robotic systems", in *Proceedings of the 2016 2nd workshop on advanced research and technology in industry applications*, vol. 5, 2016, pp. 1766–1771, doi: 10.2991/wartia-16.2016.350.

[17] W., Saab, P., Racioppo, and P., Ben-Tzvi, "A review of coupling mechanism designs for modular

reconfigurable robots," *Robotica*, vol. 37, no. 2, Feb. 2019, pp. 378–403, doi: 10.1017/S0263574718001066.

[18]   K., Gnana Sheela, P.J., Menon, S., Swetha, C.M., Vandana, R., Mendez, "Review on bio-inspired modular robotic system," S. Mohamed, T.D., Subash, (Eds.) *Materials today: proceedings, Amsterdam, Netherlands: Elsevier*, vol. 24, 2019, doi: 10.1016/j.matpr.2020.03.618.

[19]   A., Lyder, R.F.M., Garcia, and K., Stoy, "Mechanical design of Odin, an extendable heterogeneous deformable modular robot," in *IEEE/RSJ international conference on intelligent robots and systems (IROS)*, Nice, France, 2008, doi: 10.1109/IROS.2008.4650888.

[20]   G.S., Chirikjian, "Kinematics of a metamorphic robotic system," in *Proceedings of the 1994 IEEE international conference on robotics and automation*, San Diego, CA, USA, 1994, pp. 449-455 vol.1, doi: 10.1109/ROBOT.1994.351256.

[21]   K., Stoy, D.J., Christensen, D., Brandt, M., Bordignon, and U.P., Schultz, "Exploit morphology to simplify docking of self-reconfigurable robots," in Asama, H., Kurokawa, H., Ota, J. & Sekiyama, K. (Eds.) *Distributed autonomous robotic systems*, Tsukuba, Japan. Berlin/ Heidelberg, Germany: Springer. vol. 8., 2009, doi: 10.1007/978-3-642-00644-9_39.

[22]   J. W. Romanishin, K. Gilpin, S. Claici, and D. Rus, "3D M-Blocks: Self-reconfiguring robots capable of locomotion via pivoting in three dimensions," in *IEEE International Conference on Robotics and Automation (ICRA)*, Seattle, WA, USA, 2015, pp. 1925-1932, doi: 10.1109/ICRA.2015.7139450.

[23]   D., Saldana, B., Gabrich, G., Li, M., Yim, and V. Kumar, "ModQuad: the flying modular structure that self-assembles in Midair," in *Proceedings of the IEEE international conference on robotics and automation*, Brisbane, QLD, Australia. 2018, New York: IEEE, doi: 10.1109/ICRA.2018.8461014.

[24]   B., Piranda, P., Chodkiewicz, P., Holobut, S., Bordas, J., Bourgeois, and J. Lengiewicz, "Distributed prediction of unsafe reconfiguration scenarios of modular robotic programmable matter," *IEEE Transactions on Robotics*, vol. 37, no. 6, Dec. 2021, pp. 2226–2233, doi: 10.1109/TRO.2021.3074085.

[25]   M. Nisser, L. Cheng, Y. Makaram, R. Suzuki, and S. Mueller, "ElectroVoxel: Electromagnetically Actuated Pivoting for Scalable Modular Self-Reconfigurable Robots," in *International Conference on Robotics and Automation (ICRA)*, Philadelphia, PA, USA, 2022, pp. 4254-4260, doi: 10.1109/ICRA46639.2022.9811746.

[26]   Q., Song, D., Ye, Z., Sun, and B., Wang, "Motion planning techniques for self-configuration of homogeneous pivoting cube modular satellites," *Aerospace Science and Technology*, Jan. 2022, vol. 120, Art. no. 107249, doi: 10.1016/j.ast.2021.107249.

[27]   S., Hauser, M., Mutlu, A.J., Ijspeert, "Kubits: Solid-state self-reconfiguration with programmable magnets," *IEEE Robotics and Automation Letters*, vol. 5, no. 4, Oct. 2020, pp. 6443-6450, doi: 10.1109/LRA.2020.3013884.

[28]   A., Bhattacharjee, Y., Lu, A.T., Becker, and M., Kim, "Magnetically controlled modular cubes with reconfigurable self-assembly and disassembly," *IEEE Transactions on Robotics*, vol. 38, no. 3, June 2022 pp. 1793-1805, doi: 10.1109/TRO.2021.3114607.

[29]   Z., Butler and D., Rus, "Distributed planning and control for modular robots with unit-compressible modules," *Int. J. Robot. Res.*, vol. 22, no. 9, Sep. 2003, pp. 699–715, doi: 10.1177/02783649030229002.

[30]   C., Ünsal, H., Kiliççöte, P.K., Khosla, "A modular self-reconfigurable bipartite robotic system: implementation and motion planning," *Autonomous Robots*, vol. 10, Jan. 2001, pp. 23–40, doi: 10.1023/A:1026592302259.

[31]   B., Piranda, G.J., Laurent, J., Bourgeois, C., Clévy, S., Möbes, and N.L., Fort-Piat, "A new concept of planar self-reconfigurable modular robot for conveying microparts," *Mechatronics*, vol. 23, no. 7, Oct. 2013, pp. 906-915, doi: 10.1016/j.mechatronics.2013.08.009.

[32]   H., Kurokawa, K., Tomita, A., Kamimura, S., Kokaji, T., Hasuo, and S., Murata, "Distributed self-reconfiguration of m-tran iii modular robotic systems," *International Journal of Robotics Research*, vol. 27, no. 3-4, March-April 2008, pp. 373–386, doi: 10.1177/0278364907085560.

[33]   D., Rus and M., Vona, "Crystalline robots: self-reconfiguration with compressible unit modules,"

Autonomous Robots, vol. 10, Jan. 2001, pp. 107–124, doi: 10.1023/A:1026504804984.

[34] W. Y. Yang, Y. Zou, J. Huang, R. Abujaber, and K. Nakagaki, "TorqueCapsules: Fully-Encapsulated flywheel actuation modules for designing and prototyping movement-based and kinesthetic interaction," in 37th Annual ACM Symposium on User Interface Software and Technology (UIST '24). Association for Computing Machinery, New York, NY, USA, 2024, Article 98, 1–15, doi: 10.1145/3654777.3676364.

[35] M. Gajamohan, M. Muehlebach, T. Widmer and R. D'Andrea, "The Cubli: A reaction wheel based 3D inverted pendulum," in European Control Conference (ECC), Zurich, Switzerland, 2013, pp. 268-274, doi: 10.23919/ECC.2013.6669562.